Reversed Flow through a Kaplan Runner

An investigation of the flow characteristics of a Kaplan runner operating as a pump under reversed-flow conditions

By DR. R. N. KAR

PART ONE

THE pattern of flow through a conventional Kaplan turbine runner with blades made of aerofoil sections is already well known. This, however, is not the case when a Kaplan turbine runner runs as a pump, with a reversed direction of rotation and flow. The object of this investigation was to determine in general such a behaviour under reversed conditions and in particular about a tubular-type Kaplan turbine. With the flow direction reversed and moving from the sharp trailing edges towards the rounded-off leading edges of runner and guide vanes during pumping operation, as shown under alternative TP Fig. 1*d*, the aerodynamic characteristics of any single aerofoil section, and in particular that of the cascade, are almost unknown. It becomes necessary, therefore, to investigate theoretically and experimentally these aerodynamic characteristics, before one can tackle the problem of a turbine run as a pump.

If one considers only the usual small changes in vane settings the four alternatives given in Fig. 1 and Table I are possible.

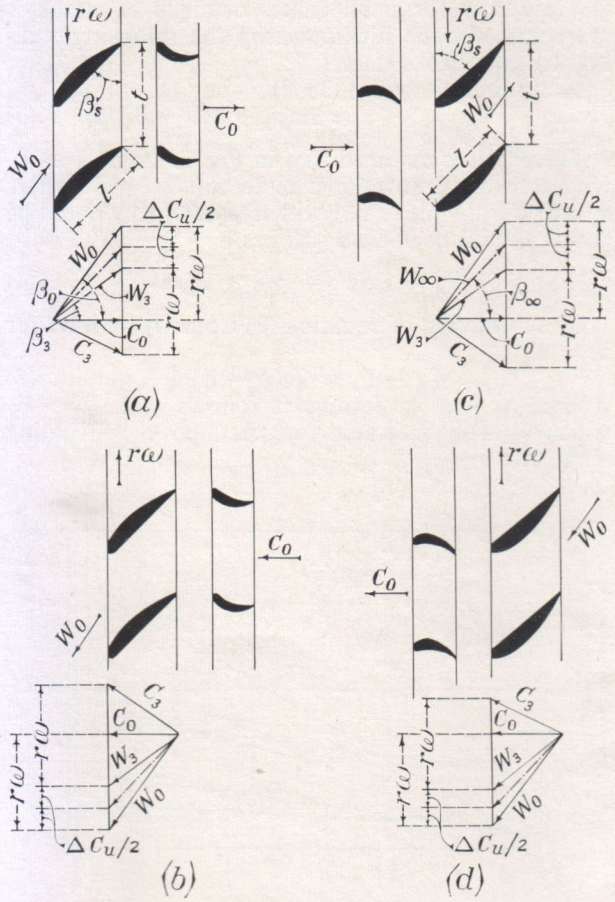

Fig. 1

The possibility of turning the vanes through 180° in alternatives TT and PP has not been considered here. The alternatives PP and TT according to Fig. 1*a* and 1*c* represent the already well-known cases, and will be referred to only for purposes of relevant comparison. The alternative TP (Fig. 1*d*) is the main theme of this investigation, and the possibility PT (Fig. 1*b*) has not been dealt with.

For investigating theoretically both a single and a cascade of stationary aerofoils under normal and reversed conditions of flow, the method proposed by Schlichting[5] has been used. The experimental work comprises measurements of aerodynamic coefficients on a single aerofoil under normal and reversed flow and on a rotating cascade represented by arrangements PP and TP, by measuring output, axial thrust, etc.

Single Aerofoil under Reversed-Flow Conditions

The question arises as to how the aerodynamic characteristics of an aerofoil are affected with reversal of flow, i.e., flow from the sharp trailing edge towards the rounded-off leading edges. According to Brown[1] theoretically the slope of lift and profile-drag curves remains unaltered for aerofoils of very small camber under reversed flow. Such an assumption cannot reasonably be justified for appreciably thick or highly cambered aerofoils. The aerofoil sections on or next to the hub of a Kaplan runner blade are appreciably thick, in order to provide the necessary high lift required for maintaining the usual constant angular momentum (Cu_3r = constant) design condition throughout the blade. So these sections cannot be treated on a thin-aerofoil basis.

The behaviour of such a highly cambered aerofoil under reversed conditions of flow is illustrated in Fig. 2 by the measurement of lift and drag coefficients through 0–360° angle of attack, on Göttingen profile No. 420[2]. Similar measurements on other aerofoils have been made by Lock and Townend[3] and Pope[4]. Some outstanding observations from these results, pertaining to reversed-flow phenomena can be summarised as below:

(*a*) Under reversed-flow conditions for same angles

TABLE I

Abbreviations	Vanes Designed for	Run as	Nature of Flow in Cascade	Direction of flow	Fig.
PP	Pump	Pump	Decelerating	Normal	1*a*
PT		Turbine	Accelerating	Reversed	1*b*
TT	Turbine	Turbine	Decelerating	Normal	1*c*
TP		Pump	Accelerating	Reversed	1*d*

of attack ($\alpha' = \alpha$) when referred to the tangent on the pressure side (see Fig. 3*a*) the gliding angle $\varepsilon' = \zeta'_W/\zeta'_A$ is always bigger than $\varepsilon = \zeta_W/\zeta_A$ under normal flow. This effect of $\varepsilon' > \varepsilon$ is more pronounced with profiles that have relatively greater camber.

(*b*) The smallest values of gliding angle ε' under reversed flow occur with positive angles of attack α'.

(*c*) There exists a positive linear relationship (Fig. 4) between $\Delta\zeta_A$ and $\Delta\zeta_W$ (the difference in the aerodynamic coefficients under normal and reversed flow) and f/l (camber-chord ratio) for small and equal positive angles of attack ($\alpha = \alpha'$).

The above experimental observations on single aerofoils indicate that an overall decrease in efficiencies of runner and guide vanes can be expected under

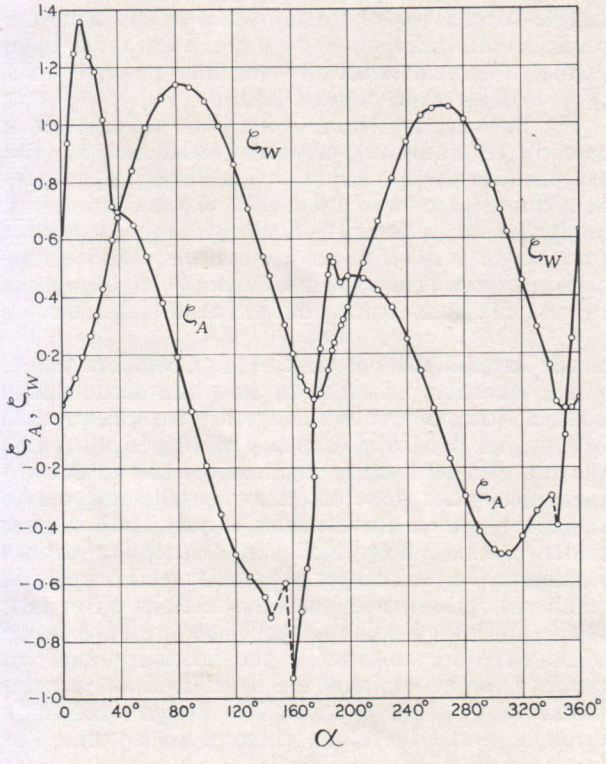

Fig. 2

reversed flow. With the changeover from turbine to pump operation it is expected that the sections with relatively smaller camber (near the outer periphery of vane) contribute less towards lowering the efficiency than the highly cambered ones at or near the hub.

Lift of an Infinitely Thin Profile (Potential theory)

The change in lift under reversed-flow conditions was theoretically determined according to Schlichting's method[5]. The lift is directly dependent on the slope of the camber line, with the result that its estimation under reversed flow does not present any difficulty so long as all the distances, etc., are referred to the other end of the camber line.

According to these calculations one gets the expressions for lift coefficients ζ_A and ζ'_A under normal and reversed flow respectively, which are dependent on the angle of attack α_s, α'_s (Fig. 3) and the geometry of the camber line. The expressions for the difference in lift coefficients under these different directions of flow have been worked out in Ref. 6 and are:

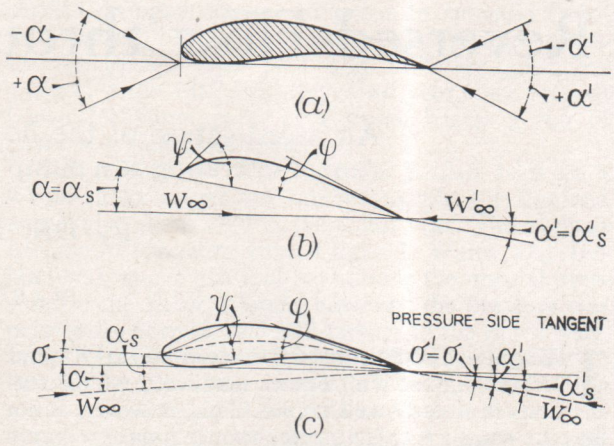

Fig. 3

$$\Delta\zeta_A = \zeta_A - \zeta'_A = K.\ 2\pi\cos\alpha \qquad ..(1)$$

$$\Delta\zeta_A = 2\pi K.\ \text{(for small values of } \alpha_s) \qquad ..(2)$$

A change in the camber f accordingly alters the constant K in these expressions. Fig. 5 shows exact relations between ζ'_A, ζ_A, $\Delta\zeta_A$ and f/l for the Göttingen profile No. 428 according to calculations in Ref. 6. The values have been determined for various f/l ratios.

A comparison of Fig. 4 or 2 and 7 with Fig. 5 clearly shows that there exists theoretically a negative difference in lift against the positive experimental values (i.e. theoretically $\zeta'_A > \zeta_A$ when the angle of attack is referred to the camber-line chord). That according to potential theory (Fig. 5) the lift under reversed flow for small values of angle of attack is more can also be illustrated by the following well-known expressions in Ref. 7:

$$\zeta_A = 2\pi\sin(\alpha_s + \psi/8 + 3\phi/8) \approx 2\pi(\alpha_s + \psi/8 + 3\phi/8) \qquad ..(3)$$

Thereby it is assumed that in Fig. 3*b* angle $\psi > \phi$. Under reversed flow for a plate with $\alpha_s = \alpha'_s$ where α_s and α'_s are measured with respect to camber-line chord, the lift coefficient will be:

$$\zeta'_A \approx 2\pi(\alpha'_s + \phi/8 + 3\psi/8) \qquad ..(4)$$

By subtraction of equation (3) from (4) we have for $\alpha_s = \alpha'_s$

$$\zeta'_A - \zeta_A \approx 2\pi(\psi - \phi)/4 \qquad ..(5)$$

Since $\psi - \phi$ is positive it follows that $\zeta'_A > \zeta_A$ which is also indicated by the above Schlichting method.

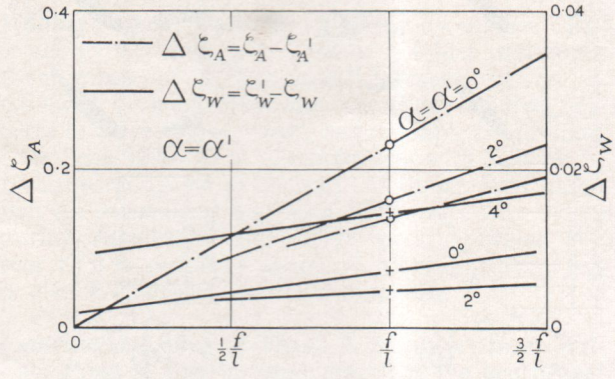

Fig. 4

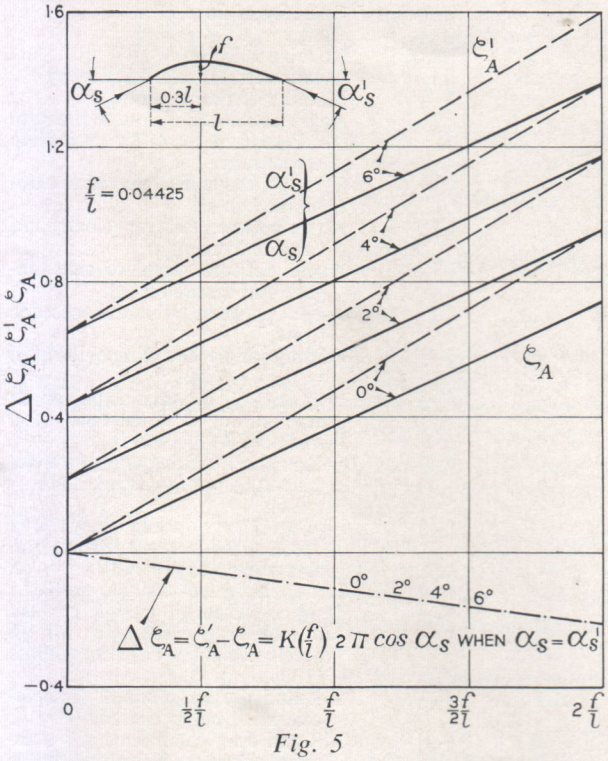

Fig. 5

Aerofoil of Finite Thickness

So far, in our calculations above, we took into account only the camber line, and neglected the aerofoil thickness. The angles of attack α'_s, α_s were also referred to the camber-line chord. Now, if one considers a profile of appreciable thickness for equal angles of attack ($\alpha = \alpha'$) referred to the pressure-side tangent as in Fig. 3*c* or 3*a*, then with normal flow direction $\alpha_s = \alpha + \sigma$.

$$\zeta_A \approx 2\pi(\alpha + \sigma + \psi/8 + 3\phi/8) \qquad ..(6)$$

Similarly under reversed-flow direction $\alpha'_s = \alpha - \sigma$. By its substitution in equation (4) and then subtracting (6) we get for $\alpha = \alpha'$

$$\zeta'_A - \zeta_A = 2\pi[(\psi - \phi)/4 - 2\sigma] \qquad ..(7)$$

Accordingly for a profile of finite thickness $\zeta'_A < \zeta_A$ when

$$\psi - \phi < 8\sigma$$

So a decrease in lift as measured experimentally under reversed-flow conditions for equal angles of attack referred to the pressure-side tangent could be partly explained by the above theoretical considerations.

Besides, under actual conditions one has to take into account that with the direction of flow reversed, a well-defined outflow condition at the rounded-off trailing edge does not exist. Actually there is a separation of fluid at the trailing edge which gives rise to a decreased circulation under reversed flow, compared with a build-up of circulation as theoretically expected.

Observations of Flow Patterns and Measurement of Pressure Distribution (Single Aerofoil)

In order to make some qualitative investigations of the drag under reversed flow, the flow around three small models (of different f/l ratio) of profile No. Gö 428 was observed in the smoke tunnel of the Institute for Fluid Mechanics (TH Munich). The pictures of the flow under reversed conditions show clearly that for small values of $+\alpha'$, separation takes place on the low-pressure side near the rounded-off nose trailing edge (normally the leading edge) which results in a relatively larger wake and thereby an appreciable increase in drag compared with normal flow. Under small negative values of α', separation occurs directly under the sharp leading edge (normally the trailing edge) which gives rise to a still greater drag. These experiments were carried out in the sub-critical range of Reynolds number. $Re = lW/\nu = 100$, so that it can only represent qualitatively a particular case.

Next a model of Göttingen profile No. 428* (0·7 m span and 0·3 m chord length with 29 pressure tappings) was tested in the wind tunnel (TH Munich) under

* This profile was chosen because the same was employed for the model-turbine runner blade.

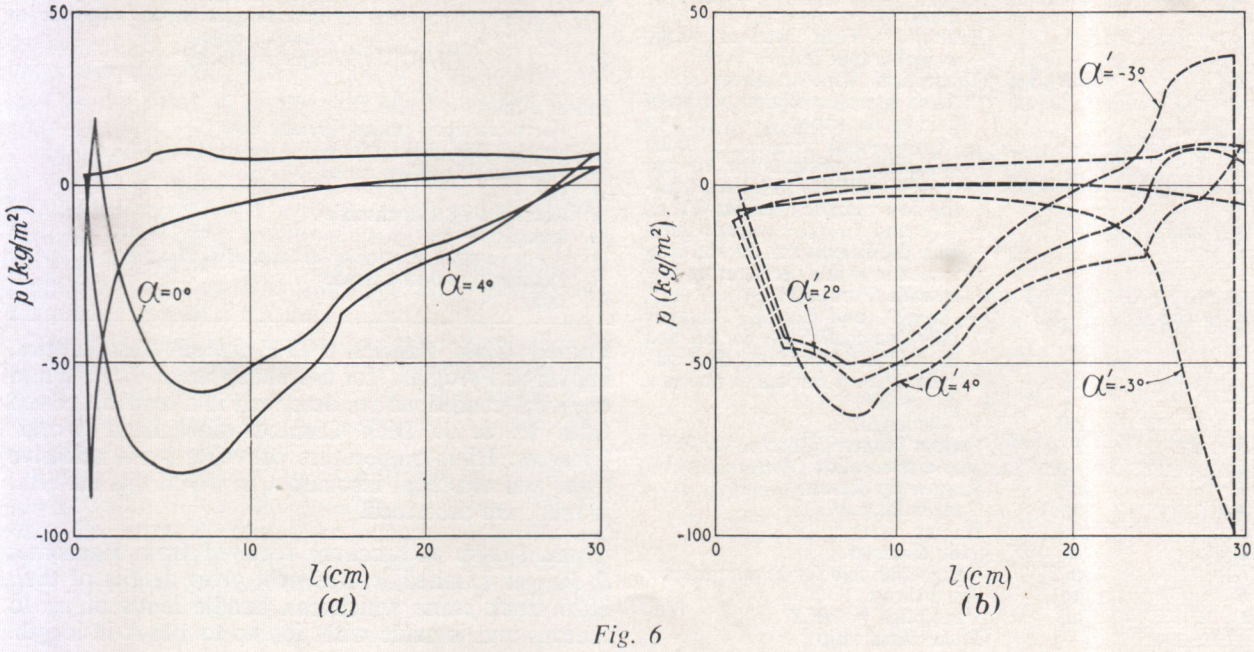

Fig. 6

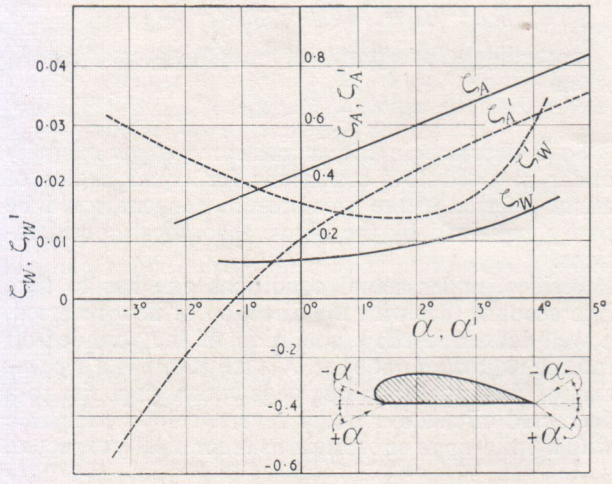

Fig. 7

normal and reversed-flow conditions for small angles of attack. The approach wind velocity was about 30 m/sec and the model carried two end plates to suppress end flow effects. These pressure measurements are represented in Fig. 6*a* and 6*b*. While as, for a small positive value of α', small low-pressure peaks are usually present, there occur low-pressure peaks of considerable magnitude (thereby indicating a danger of cavitation) for negative values of α' as shown in Fig. 6*b* ($\alpha' = -3°$). By graphical integration the lift and drag coefficients were determined from the pressure measurements as shown in Fig. 7. It is clear from this that for equal angles of attack (referred to pressure-side tangent) under normal and reversed flow, there is an appreciable increase in drag and decrease in lift.

(To be continued)

SYMBOLS AND UNITS

A	[kg]	Lift
a_0	[m]	Guide vane opening
c	[m/s]	Absolute velocity
d	[m]	Maximum profile thickness
f	[m]	Profile camber
g	[m/s²]	Acceleration due to gravity
H	[mkg/kg]	Pumps—Total head or energy produced Turbines — Total head or energy available (put in)
H_{th}	[mkg/kg]	Theoretical work or energy either taken away or offered per kg of fluid by the vanes
K_{AB} and K_{WB}	[—]	$= \zeta_{AB}/\zeta_A$ and ζ_{WB}/ζ_W, cascade influence coefficients for lift and drag respectively in an accelerating flow cascade (Turbine TT)
K_{AV} and K_{WV}	[—]	$= \zeta_{AV}$ and ζ_{WV}/ζ_W, cascade influence coefficients for lift and drag respectively in a decelerating flow cascade (Pump PP)
K'_{AV} and K'_{WV}	[—]	$= \zeta'_{AV}/\zeta'_A$ and ζ'_{WV}/ζ'_W, cascade influence coefficients for lift and drag in a decelerating flow cascade when a turbine is run as a pump (TP)
l	[m]	Profile length
N	[PS]	Output in metric horsepower
n	[r.p.m.]	Speed of rotation r.p.m.
R	[m]	Runner tip diameter $= D/2$
$R\omega$	[m/s]	Tangential velocity
r	[m]	Radius
$2r_N$	[m]	Hub diameter
$r\omega$	[m/s]	Tangential velocity at any radius r
S	[kg]	Axial thrust
t	[m]	Vane pitch $= 2\pi r/Z$
t/l	[—]	Pitch chord ratio
V	[m³/s]	Quantity of flow
W	[kg]	Drag
w	[m/s]	Relative velocity
w_∞	[m/s]	Mean vectorial relative velocity
Z	[—]	Number of runner vanes
α	[°]	Angle of attack referred to pressure side tangent chord for an infinite aspect ratio
α_s	[°]	Same as above but referred to camber line chord
β	[°]	Angle between relative velocity and cascade front
β_s	[°]	Angle between pressure side tangent and cascade front
β_∞	[°]	Angle between W_∞ and cascade front
ε	[—]	Gliding angle for single aerofoil $= \zeta_W/\zeta_A = \tan\varepsilon$
ε_B	[—]	$= \zeta_{WB}/\zeta_{AB}$, Gliding angle for an accelerating flow cascade of a Turbine (TT) $= \tan\varepsilon_B$
ε_V	[—]	$= \zeta_{WV}/\zeta_{AV}$, Gliding angle for a decelerating pump cascade (PP) $= \tan\varepsilon_V$
ε'_V	[—]	$= \zeta'_{WV}/\zeta'_{AV}$, Gliding angle for a decelerating cascade turbine run as a pump (TP) $= \tan\varepsilon'_V$
ζ_A	[—]	Lift coefficient of a single profile
ζ_W	[—]	Drag coefficient of a single profile
ζ_{AB} and ζ_{WB}	[—]	Lift and drag coefficients for an accelerating flow cascade, turbine (TT)
ζ_{AV} and ζ_{WV}	[—]	Lift and drag coefficients for a decelerating pump cascade (PP)
ζ'_{AV} and ζ'_{WV}	[—]	Lift and drag coefficients for a decelerating cascade turbine run as a pump (TP)
$\Delta\zeta_A$	[—]	Difference in lift coefficients $\zeta_A - \zeta'_A$ under normal and reversed flow for same angles of attack ($\alpha = \alpha'$) referred to pressure side tangent
$\Delta\zeta_W$	[—]	Difference in drag coefficients $\zeta'_W - \zeta_W$
η	[—]	Overall efficiency
η_h η_{VL}	[—]	Hydraulic and runner vane efficiencies respectively
ν	[m²/s]	Kinematic viscosity
ρ	[kgs²/m⁴]	Density
σ	[°]	Angle between pressure side tangent and camber line chord $= \alpha_s - \alpha$
ϕ	[°]	Angle between the camber line chord and tangent to camber line at the entrance edge
ψ	[°]	Angle between camber line chord and tangent to camber line at the exit edge
ω	[1/s]	Angular velocity

Indices used

'	For a condition under reversed flow
0	Suction side of the runner
3	Pressure side of the runner
A	Lift
B	Accelerating flow cascade
L	Runner
u	A component of velocity in tangential direction
V	Decelerating flow cascade
W	Drag

Coated Glass Fabrics. PTFE-coated glass fabrics, known as Pyroglass, for use under severe heating and chemical conditions are described in a leaflet received from R. & J. Dick Limited, Greenhead Works, Glasgow. High-temperature conveyor belts, adhesive tapes and electrical insulation, in which this material is used, are described.

Truck Crane. A brochure received from Ransomes & Rapier Limited, of Ipswich, gives details of their 2020 truck crane which can handle loads of up to 20 tons and is made with jibs up to 100 ft in length.